Behavioral/Cognitive

Vestibular Function Drives Gaze Stability in Locomoting Macaques

Oliver R. Stanley,[1] Rui-Han Wei,[1] Skyler Thomas,[1] and Kathleen E. Cullen[1,2]
Departments of [1]Biomedical Engineering and [2]Otolaryngology-Head and Neck Surgery & Neuroscience, Johns Hopkins University, Baltimore, Maryland 21205

Stable gaze is essential for effective navigation, yet during locomotion each stride generates phasic head movements that can destabilize the visual scene. The vestibular system is well positioned to counter these disturbances by sensing head motion and rapidly generating reflexive compensatory eye movements, but its specific contribution to gaze stabilization during locomotion is not well understood. To directly test the vestibular system's contribution during walking, we compared gait and gaze kinematics in male and female rhesus macaques with normal vestibular function and those with chronic bilateral vestibular loss (BVL) during treadmill walking at multiple speeds and during overground locomotion. We found that BVL animals showed systematic gait abnormalities, including markedly increased gait variability across conditions. Gaze stabilization deficits were equally pronounced: normal monkeys effectively stabilized gaze across conditions, whereas BVL animals exhibited reduced and more variable eye movements that failed to compensate for head motion. Vestibular loss increased the magnitude of reorienting eye movements, consistent with an increased tolerance for gaze position error. Extending established oculomotor models to incorporate intrinsic noise and elevated error thresholds reproduced these behavioral signatures, revealing that chronic vestibular loss drives a fundamental recalibration of gaze control strategies. Together, these findings demonstrate that vestibular input provides a central scaffold for stabilizing gaze and gait during natural locomotion and establish essential behavioral benchmarks for future neural, rehabilitative, and prosthetic interventions.

Key words: **gaze; nonhuman primate; oculomotor; sensorimotor; vestibular**

Significance Statement

Locomotion generates rhythmic head movements that must be compensated to maintain visual stability, yet the contribution of vestibular signals to gaze stabilization during natural primate locomotion has not been established. Here, we quantified gaze and gait behavior in rhesus macaques with chronic bilateral vestibular loss during treadmill and overground walking. Vestibular loss increased stride-to-stride gait variability, reduced the consistency of compensatory eye-head coupling, and altered the magnitude of gaze-reorienting movements. Computational modeling further showed that these behavioral changes are consistent with the presence of sensorimotor noise and elevated gaze-error tolerance. Together, these findings demonstrate that vestibular signals provide a central scaffold for stabilizing gaze during locomotion and reveal how oculomotor strategies reorganize following sensory loss.

Introduction

Coordinating head and eye movements to stabilize gaze is essential for navigation and sensorimotor coordination. Although vision provides the high-resolution spatial information needed to guide behavior (Srivastava et al., 2018), locomotion introduces rapid, phasic head movements that require compensatory eye movements to preserve ongoing visual stability. These disturbances follow gait-linked patterns across species (Solomon and Cohen, 1992; Cromwell et al., 2004; Zubair et al., 2019). Thus, to maintain perceptual stability, the nervous system must generate rapid oculomotor responses that offset head motion. Because visual processing is too slow to compensate for step-linked dynamics, visual stability depends on fast vestibular reflexes (Goldberg et al., 2011), including vestibulo-collic and vestibulo-spinal pathways that stabilize the head and the vestibulo-ocular reflex (VOR), which counter-rotates the eyes during head motion. In healthy subjects, these reflex pathways integrate eye, head, and body movements into a unified sensorimotor system that stabilizes gaze

Received March 9, 2026; revised May 14, 2026; accepted June 18, 2026.
Author contributions: O.R.S., R-H.W., and K.E.C. designed research; O.R.S. and R-H.W. performed research; O.R.S. and S.T. analyzed data; O.R.S. and K.E.C. wrote the paper.
This work was supported by the National Institutes of Health grants R01DC002390, R01DC018061, T32DC000023 (K.E.C.), and F31DC021106 (O.R.S.) as well as a Postdoctoral Research Accelerator Award and a Kavli Neuroscience Discovery Institute Distinguished Postdoctoral Fellowship (R.H.W.). We thank Dale Roberts for his technical support and Dr. Robyn Mildren for feedback regarding statistical methods.
The authors declare no competing financial interests.
Correspondence should be addressed to Kathleen E. Cullen at kathleen.cullen@jhu.edu.
This paper contains supplemental material available at: https://doi.org/10.1523/JNEUROSCI.0423-26.2026
https://doi.org/10.1523/JNEUROSCI.0423-26.2026

during locomotion (Imai et al., 2001; Matthis et al., 2018; Zubair et al., 2019).

When vestibular input is lost, the control architecture that supports this coordination is fundamentally disrupted. Head kinematics become irregular (Zobeiri et al., 2021; Millar et al., 2023), visual stability is reduced (Anson et al., 2017), and individuals experience major deficits in balance, locomotion, and quality of life (Schniepp et al., 2012; Agrawal et al., 2013; Wuehr et al., 2016; McCrum et al., 2019). Yet the consequences of chronic bilateral vestibular loss (BVL) for primate gaze control during locomotion have never been directly quantified. This gap is particularly important because nonhuman primates rely on foveal vision and share homologous oculomotor circuitry with humans, allowing direct mechanistic translation to vestibular disease.

To determine how vestibular loss alters locomotor gaze control, we must consider the complementary oculomotor mechanisms that normally support this coordination. Slow phases are smooth, compensatory eye movements—primarily driven by the VOR—that counteract head motion and reduce retinal slip. Because the eye has a finite range in the orbit, compensatory movements must be periodically reset by rapid eye movements. Rapid movements include quick phases and saccades, both generated by shared burst generator circuitry (Corneil et al., 2002; Scudder et al., 2002; Takahashi and Veale, 2023). During locomotion, smooth stabilization and rapid gaze shifts interact continuously to maintain visual stability and enable exploration. Given this dual-mode control architecture, we predicted that BVL would impair gait and slow-phase gaze stability due to the absence of vestibular reflex drive (Cullen, 2019). In contrast, the impact on rapid gaze shifts was less predictable. Under one hypothesis, they might increase in frequency or amplitude to provide more effective corrections for unstable head motion. Alternatively, head instability might make reorientation less effective for placing the visual axis on-target and thus lead to reduced frequency to avoid wasted effort.

Despite extensive work on vestibular contributions to gaze stabilization in stationary or head-fixed conditions, its role during locomotion remains unresolved, particularly in primates. To address this gap, we quantified locomotor gaze control in rhesus macaques with chronic BVL and vestibular-intact controls during treadmill and overground walking. Increasing treadmill speed produced faster strides and higher slow-phase gaze velocities in both groups. However, BVL animals exhibited greater stride variability, elevated slow-phase gaze velocities, and reduced and more variable eye-head gains across conditions, consistent with degraded gaze stabilization. They also generated larger gaze-reorienting movements during treadmill locomotion, although this pattern reversed during overground walking, where reorientation magnitudes were reduced relative to controls. Although gaze control deficits persisted overground, BVL animals partially improved stabilization during self-paced walking, indicating that locomotor context shapes vestibular-dependent gaze control. Computational modeling further showed that the presence of sensorimotor noise and relaxed error thresholds account for the variability in slow-phase gain and gaze reorientation. Together, these findings establish quantitative behavioral benchmarks linking vestibular dysfunction to sensorimotor control principles and demonstrate that chronic vestibular loss does not simply degrade gaze stability, but reorganizes the strategies governing eye-head coordination during self-motion.

Materials and Methods

Data processing and statistical analysis were performed with MATLAB R2024b (MathWorks). For our data analysis, we define a spatial coordinate frame centered at the middle of the walkway, with the x-axis parallel to the short axis of the walkway, y-axis parallel to the long axis, and z-axis parallel to gravity. The x-axis (lateral) was positive to the monkey's left when on the treadmill, the positive y-axis (fore-aft) was along the direction of forward treadmill walking, and the z-axis (vertical) was positive downward. The directions of rotational axes followed the right-hand rule (i.e., yaw rotation was positive if the animal turned clockwise seen from above). Pairwise post hoc comparisons were performed via Holm–Bonferroni multiplicity correction. Grouped data are presented as bar plots indicating median (central line), quartiles (central bar), and 95th percentile (whiskers). For individual monkeys, data are presented in dot plots containing a single data point for each event of interest (either a single stride or single gaze reorientation).

Animal care and use. Five monkeys (*Macaca mulatta*: three females, two males) were used in this study. All experimental procedures were approved by the Johns Hopkins University Animal Care and Use Committee (protocol PR22M34 and PR25M286) and were carried out in accordance with the National Institutes of Health Guide for the Care and Use of Laboratory Animals (NIH Publications No. 8023, revised 2011). Under anesthesia, animals were implanted with titanium skulls posts to enable mounting sensors to the head, secured using titanium screws and dental acrylic. All animals recovered at least 2 weeks from implantation before any training or experiments. Three animals (G, J, N) subsequently underwent bilateral vestibular ablation via intratympanic injection of gentamicin. Efficacy of semicircular canal function loss was confirmed via VOR testing in yaw and pitch (gain of <0.1 during sinusoidal rotation in the dark). While intratympanic gentamycin is reported to impact otolith function (Helling et al., 2007; Yang et al., 2010) while preserving hearing (Scarpa et al., 2024), we did not quantitatively test for these functions. However, BVL animals remained responsive to conspecific vocalizations as well as to verbal cues during experiments. Post-BVL acclimation and behavioral training in the experimental apparatus began after at least 1 month of recovery (1 month for Animals J and N; ~10 years for Animal G) and, as described below, lasted for at least 2 months. Behavioral data for the current study were thus collected only after at least 3 months post-lesion, a time period sufficient to allow central adaptation and sensory substitution (Dichgans et al., 1973; Sadeghi et al., 2012). For Animal J, behavioral data was obtained prior to induction of BVL, and training and data collection were then repeated after recovery. Animals G and N did not have exposure to the experiment with normal vestibular function.

Behavior training. All monkeys were trained to walk quadrupedally (Fig. 1*A*) either on a linear walkway (~140″ × 20″) or on a treadmill placed on that walkway (approx. 16″ width). As we described previously (Wei et al., 2026), these setups were of sufficient size to avoid limiting stride length or width and consisted of thin rubber over metal base, providing comparable support surfaces. The ends of the track were mounted on a pivot that when released allowed the experimenter to rotate the monkey by 180° for repeated trips along the track. Walkway height was adjusted to a comfortable level for each animal at the start of each behavior session. Animals were equipped with a collar which could be fixed to a modified primate chair suspended from overhead rails parallel to the walkway. A braking mechanism on the rails allowed the maintenance of chair position necessary for treadmill walking, while the chair could move on low-friction bearings during overground locomotion when the brake was disengaged. Head and body orientation and position, as well as visual exploration and fixation behavior, were otherwise unrestrained.

Animals were acclimated to the behavioral apparatus via short sessions during which they were provided preferred food and liquid rewards before being returned to housing. During overground walking, monkeys traversed the walkway at a self-selected pace to obtain rewards. Animals were encouraged to maintain a locomotor speed of ~1.7 MPH by withholding reward when traversal took 5 s or longer. An overground walking session comprised at least five round-trips of the track. Treadmill

walking sessions comprised 15 s of continuous walking at several speeds (0.8, 1.1, 1.4, 1.7 MPH). Each animal was trained for a minimum of 2 months before data were collected. After each locomotor trial, preferred food (dry fruit, nuts) or liquid (juice) were given as rewards.

Markerless motion capture. Four video cameras (Blackfly S BFS-U3-13Y3M; FLIR) were placed around the walkway to enable recording of animals' gaits in 3D via markerless feature tracking. Cameras recorded synchronized frames at 100 Hz. Synchronization pulses were also transmitted to an analog recording system (OmniPlex, Plexon) for later alignment. DeepLabCut (Mathis et al., 2018), an open-source deep learning software package enabling markerless pose estimation, was then used to extract the animals' 3D posture (x, y, z coordinates of bilateral shoulder, elbow, wrist, fingertip, hip, knee, ankle, and toe tip). These data were used to identify, and align data to, gait cycles. Gait cycles were segmented based on left forelimb elevation, defined by the vector between the shoulder and wrist relative to the world vertical, with stance phase onset at the peak elevation angle (Fig. 1*B*).

Head and eye tracking and processing. An analog inertial measurement unit (IMU; Model 634, TE Connectivity) to record head angular velocity and linear acceleration at 1 kHz and retroreflective marker system (Vagvolgyi et al., 2022) to track head orientation and position were attached to the animal's implant. A dedicated camera was fixed to the modified primate chair to track the head (100 Hz, synchronized to motion capture cameras). A 20 Hz low-pass filter (Butterworth, fourth order) was applied head velocity data. For each animal, we designed and 3D printed a video oculography camera holder which could be affixed to the implant to position a visually transparent infrared mirror (#43-843; Edmund Optics) directly in front of the left eye and reflect its image to a 200 Hz camera (Firefly FFY-U3-04S2M-S; FLIR). The camera lens was equipped with an infrared-pass filter, and infrared LEDs were positioned to achieve consistent illumination of the eye. Acquired images were analyzed by custom software which identified the position of the pupil center. Calibration from pixels to degrees was achieved by first training animals to make saccades between laser point targets placed at ±15° horizontally, during which a simple ratio between pixels and angle was manually tuned on-line to allow the animal to obtain rewards from an automated juice delivery system. Offline, to account for the geometry of the eye, distance moved by the pupil between the targets was used to calculate the radius of the eye in pixels, from which we calculated angular position using a custom MATLAB script to find the intersection between a sphere of the calculated radius and a ray extending from the image plane toward that sphere at the coordinates of the pupil center. Pupil position was written to a local file as well as recorded to an analog input channel (OmniPlex, Plexon) via a DAQ (2770-782604-01-ND, National Instruments) alongside separate synchronization pulses for later alignment with other data streams.

Eye position was first low-pass filtered (Butterworth, fourth order) at 100 Hz for desaccading. Samples within 30 ms of a blink were removed to avoid interference of the eyelid on calculated pupil position, and strides in which blinks or otherwise lost tracking occupied >40% of the gait cycle were excluded from our analyses. Reorientations were identified as periods where the vector sum of horizontal and vertical eye velocity exceeded the vector sum of yaw and pitch head velocity by at least 50 degrees per second. If the vertical or horizontal component of eye movement exceeded this threshold relative to pitch or yaw head motion individually, the event was considered for computational model analysis of vertical or horizontal quick phases (see below). Eye position was then synchronized to analog head velocity and upsampled to 1 kHz. Position during identified slow phases was then filtered with the same 20 Hz filter as head velocity and differentiated to obtain slow-phase eye velocity. Gaze velocity in the pitch and yaw axes was calculated by separately summing head and eye velocities in those axes.

Linear mixed-effects modeling. To assess the effect of vestibular loss and walking condition while accounting for within-animal and within-group correlations, statistical differences were identified by fitting linear mixed-effects models (LMMs; Boisgontier and Cheval, 2016) on data from each stride from all animals compiled into a single table. These models were parameterized as follows:

$$\text{Outcome} \sim 1 + \text{Condition} + \text{BVL} + \text{Condition} * \text{BVL} + (1|\text{Subject}) + (1|\text{BVL}),$$

where "Outcome" represents each parameter of interest [stride duration, gaze mean absolute velocity (MAV), gain], "Condition" and "BVL" are categorical variables, "Condition*BVL" is an interaction term, and "(1|Subject)" and "(1|BVL")" are animal- and group-specific intercepts. Our model thus included two fixed effects, two random effects, and one interaction effect. Models were fit using the "fitlme" function in the Statistics and Machine Learning Toolbox of MATLAB 2024b. This formulation was modified slightly in analysis of coefficient of variation (CV) and quick-phase ("Q") thresholds due to grouping of data across conditions:

$$\text{Outcome} \sim 1 + \text{BVL} + (1|\text{subject}) + (1|\text{BVL}).$$

Results are presented as boxplots containing median (center line), interquartile range (box), and whiskers extending to the 95th percentile of the group data.

Phase locking. As described by Kajikawa and Hackett (2005), we calculate a phase locking index (PLI) between the onset of gaze reorientation events and the gait cycle by comparing the entropy of the true distribution against the entropy of reshuffled interevent interval distributions. Specifically, after grouping N reorientation onset phases into $M = 36$ bins, we calculate a PLI for each animal in each walking condition as follows:

$$\text{PLI} = 1 - \frac{E_{\text{True}}}{E_{\text{Max}}},$$

$$E_{\text{Max}} = \log_2(m),$$

$$E_{\text{True}} = \sum_{m=1}^{M} P_{\text{m}} * \log_2(P_{\text{m}}),$$

where P_{m} is the fraction of events falling within bin m. Significance was tested by comparing PLI values against bootstrapped distributions of reshuffled interphase intervals between reorientation events.

Slow-phase modeling. We used a well-established VOR pathway model previously applied by our group (Mackrous et al., 2020) in conjunction with a parallel OKR pathway model (Robinson, 2022) to generate predicted slow-phase eye movements in response to the head velocity recorded during overground locomotion. The following transfer functions were employed in Simulink (MathWorks); parameter values are specified below:

$$\text{SCC} + \text{Afferents} : \frac{(s * T_{\text{Lead}} + 1) * (s * T_{\text{C}_{\text{Long}}}) * (s * T_{\text{Adapt}})}{(s * T_{\text{C\_Long}} + 1)(T_{\text{C\_Short}} * s + 1)(s * T_{\text{Adapt}} + 1)},$$

$$\text{Afferent Noise} : N(\mu = 0,\ \sigma = 10),$$

$$\text{Vestiblar Nuclei} : \frac{T_{\text{VOR}}\ (s * T_{\text{C\_Long}} + 1)}{T_{\text{C\_Long}}(s * T_{\text{VOR}} + 1)},$$

$$\text{Neural Integrator} : \frac{s * T_{E\_\text{Long}} + 1}{s} * e^{-s * \tau 1},$$

$$\text{OKR} : \frac{G_{\text{OKR}}}{s * T_{\text{OKR}} + 1} * e^{-s * \tau 2},$$

$$\text{Plant}: \frac{s}{(T_{E\_\text{Long}} * s + 1)(T_{E\_\text{Short}} * s + 1)},$$

- s is the Laplace domain variable
- $T_{\text{Lead}} = 0.049$ s, $T_{C\_\text{Short}} = 0.0027$ s, $T_{C\_\text{Long}} = 5.7$ s, and $T_{\text{Adapt}} = 80$ s are time constants representing semicircular canal cupulae and vestibular afferent dynamics (Fernandez and Goldberg, 1971)
- $T_{\text{VOR}} = 20$ s is the VOR time constant
- $T_{E\_\text{Long}} = (0.15, 0.24)$ sec and $T_{E\_\text{Short}} = (0.02, 0.013)$ sec are time constants describing the neural integrator and plant dynamics (Robinson, 2022), and $\tau 1 = 7$ ms is a delay between head motion and vestibular-driven eye movement.
- $T_{\text{OKR}} = 20$ s, $G_{\text{OKR}} = [(T_{\text{VOR}}/T_{C\_\text{Long}}) - 1] \sim 2.5$ is the visual input gain, and $\tau 2 = 100$ ms represents the longer lag between visual input and vision-driven eye movement

Quick-phase modeling. The quick-phase extension of the model was adapted from the nystagmus burst generator framework originally described by Chun and Robinson (Chun and Robinson, 1978). In order to effectively fit quick-phase parameters for each animal, the Simulink approach used above was prohibitively slow. Instead, it was necessary to apply a more computationally efficient approach. Specifically, a second-order discrete-time state-space dynamical system, which included both slow- and quick-phase subsystems, was implemented using custom MATLAB scripts. The system operates in two distinct states: a slow-phase state where subthreshold head movements generate only compensatory eye movements and a quick-phase state where suprathreshold stimuli trigger reorienting quick-phase eye movements.

Each block of the slow-phase subsystem is computed using forward state-space equations of the form:

$$x[t+1] = \mathbf{A} * x[t] + \mathbf{B} * u[t]$$
$$y[t] = \mathbf{C} * x[t] + \mathbf{D} * u[t],$$

with input u, internal state x, and output y. A set of matrices **A**, **B**, **C**, **D** implement the transfer function for each block, as described above, the output of which is then passed forward to subsequent blocks.

The quick-phase extension augments this slow-phase architecture by introducing quick-phase control mechanisms triggered by comparing "center of interest" (COI) estimates derived from semicircular canal signals to eye position estimates from the neural integrator block. As developed by Chun and Robinson, quick-phase generation is controlled by two principal modules. The "burst amplitude" module determines saccade target position based on estimated head orientation from canal afferents. The burst trigger module compares the model's internal head and eye position estimates and initiates a switch (yellow box) out of slow phase when this difference exceeds a quick-phase ("Q") threshold. This Q-threshold varies linearly with head velocity but is limited by minimum and maximum values.

To determine the parameters of these modules, we first identified reorienting eye movements in which the signs of eye vertical or horizontal displacement differed from those of head pitch and yaw displacement. These were assumed to be saccadic in nature and were discarded. For each of these remaining reorienting movements, we extracted eye position at termination and corresponding head velocity values at initiation. For each animal and condition, parameters for the COI block were optimized by minimizing the mean squared error between predicted values and observed eye positions at quick-phase endpoints using the "fmincon" function with sequential quadratic programming from the Optimization Toolbox in MATLAB 2024b.

For each event, we calculated gaze position error as the difference between the predicted COI using these animal-specific fitted parameters and measured eye position at the sample immediately preceding movement onset. The Q-threshold parameter, which determines when positional error triggers a corrective movement, was estimated separately for pitch and yaw axes (van Gisbergen et al., 1985) within each animal across all locomotor conditions by computing the deviation between eye position at event onset and estimated COI based on the above-fit parameters.

Once triggered, the burst generator produces velocity commands scaled proportionally to the magnitude of position error. As the quick phase progresses and error decreases, burst amplitude diminishes toward zero, ensuring smooth termination of the eye movement. To prevent high-frequency oscillations that can occur in high amplitude switching-systems, we implemented a hysteresis algorithm to ensure smooth transitions between quick and slow states. While the Q-threshold was tuned separately per axis to accommodate axis-specific dynamics, the fundamental architecture and controller are identical across both axes ensuring a unified mechanism for slow- and quick-phase transitions.

Results

Behavioral data were recorded from rhesus macaques with normal vestibular function and from animals with chronic BVL during locomotion under multiple conditions. To determine how vestibular loss alters locomotor gaze control, animals walked either on a treadmill at several speeds or overground along a linear walkway, while three-dimensional limb kinematics, six-degree-of-freedom head motion, and monocular eye movements were recorded simultaneously (Fig. 1*A*). This design enabled parallel assessment of gait dynamics and gaze control across externally paced treadmill walking as well as more natural self-paced overground locomotion. Limb and gaze kinematics were examined as a function of treadmill speed and compared between treadmill and overground walking at matched speeds to probe the influence of locomotor control mode. Limb movements were quantified using stride duration, whereas gaze control in both pitch and yaw axes was characterized by slow-phase eye velocity and eye-head velocity gain. Stride-to-stride variability was assessed using the coefficient of variation for each measure. Rapid gaze-reorienting eye movements were further quantified in terms of frequency and magnitude. Finally, to relate observed behavioral differences between normal and BVL animals to underlying control mechanisms, an established computational model of oculomotor control was applied and extended to incorporate intrinsic sensorimotor noise.

Limb kinematics scale normally with speed but exhibit increased variability after vestibular loss

To first assess the underlying locomotor behavior during which gaze control is expressed, we quantified limb kinematics across locomotor conditions. Behavioral signals were analyzed relative to the gait cycle, aligned to stance onset of the left forelimb, to provide a common temporal reference across conditions (Fig. 1*B*). Gait cycles were identified from the elevation angle of the left forelimb, which peaked at stance onset (Courtine et al., 2005). Gait cycle-averaged limb trajectories scaled smoothly with treadmill speed (TM 0.8-1.7 MPH), as illustrated for an example animal in Figure 2*A*. In both groups, stride duration on the treadmill declined with increasing speed and was consistently lower in BVL animals (Fig. 2*B*, right; all $p < 1 \times 10^{-20}$; Table 1). Thus, the basic effect of speed on stride duration was largely preserved. At matched speeds, overground walking revealed clear context-dependent differences in limb kinematics relative to treadmill locomotion (Fig. 2*A*, compare orange and dark blue traces). While both groups exhibited longer stride durations during overground locomotion ($p = 1.7 \times 10^{-25}$, 1.3×10^{-88} for normal, BVL), stride duration was markedly increased in BVL animals relative to controls ($p = 6.5 \times 10^{-105}$).

Notably, beyond these changes in mean stride duration, vestibular loss was associated with a robust increase in stride-to-stride duration variability. This was quantified by computing the CV (standard deviation divided by mean) for each

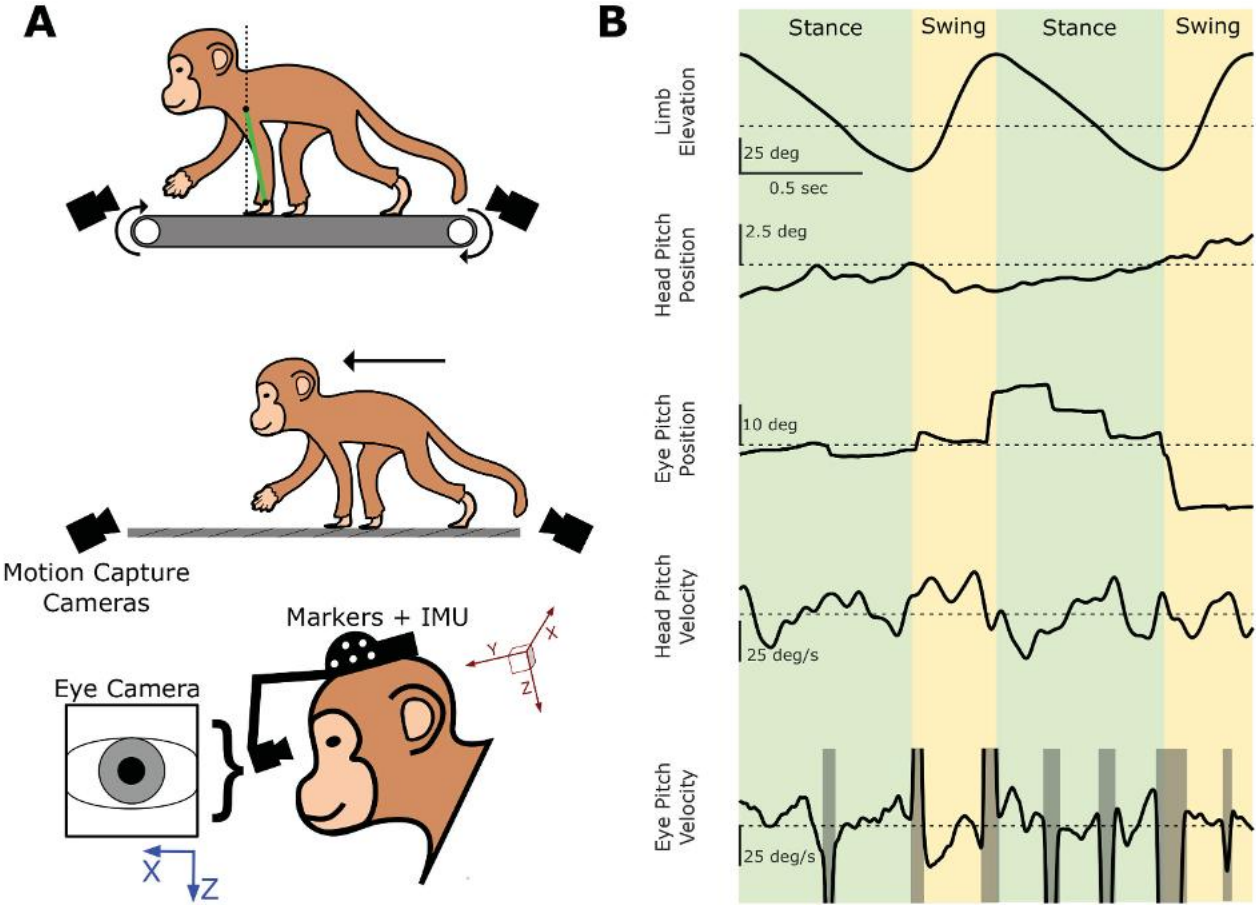

Figure 1. Illustration of data collection. ***A***, Behavioral data were recorded from rhesus macaques walking either on a treadmill or along a walkway while eye and head movements were recorded. Postural data were obtained from synchronized cameras around the behavioral apparatus. Gait cycles were segmented based on left forelimb elevation, computed using the vector from shoulder to wrist relative to world vertical (green line). ***B***, Sample data from two gait cycles from a vestibular-normal animal. Peaks correspond to stance onset (green boxes) and swing end (yellow boxes). Gaze-reorienting eye movements are denoted by gray bars overlaying eye velocity (bottom row).

animal in each condition. Pooled across all conditions, CV was significantly higher in BVL animals (Fig. 2*C*; $p = 1.4 \times 10^{-7}$). Individual-animal limb kinematic measures are shown in Figure S1. Together, these results show that vestibular loss preserves speed-dependent scaling of limb kinematics while increasing stride-to-stride variability. We next asked how these locomotor changes influenced gaze stabilization during walking.

Vestibular loss impairs slow-phase gaze stabilization during locomotion

Having established that vestibular loss impacts consistency of gait duration without substantially altering its mean, we next examined gaze behavior during locomotion by analyzing slow-phase gaze velocity computed from the sum of head and eye motion after removing rapid gaze reorientations (see Materials and Methods). Figure S2 illustrates these differences by directly overlaying eye and head velocity traces for Monkey J before and after BVL. Notably, after BVL, compensatory eye movements diminish in amplitude and become ineffective. In normal animals walking on the treadmill, slow-phase eye movements counteracted head motion in both pitch and yaw over the course of the gait cycle. This resulted in net slow-phase gaze velocities closer to zero (i.e., better compensation; Fig. 3*A*, Fig. S3*A*; solid blue traces). Following vestibular loss, slow-phase gaze motion increased markedly (dashed blue traces). To quantify this difference, we calculated the mean absolute velocity (MAV) of gaze in each axis for each stride, which equally weights net motion in either direction. We observed significantly higher gaze MAV in BVL animals for both axes (pitch, Fig. 3*B*; yaw, Fig. S3*B*; all $p < 1 \times 10^{-20}$; Table 1). In both groups, gaze MAV increased with treadmill speed, indicating that gaze stabilization became progressively more challenging as locomotor demands increased. During overground walking, gaze MAV again remained significantly higher in BVL animals for both pitch and yaw ($p = 2.1 \times 10^{-9}$ and $p = 9.9 \times 10^{-46}$, respectively), but the relationship between locomotor context and gaze stability differed across groups. In normal animals, MAV increased during overground walking relative to treadmill walking at 1.7 MPH ($p = 1.5 \times 10^{-2}$ for pitch; $p = 1.0 \times 10^{-2}$ for yaw), whereas MAV in BVL animals was reduced in the overground condition ($p = 7.3 \times 10^{-18}$ for pitch; $p = 2.2 \times 10^{-26}$ for yaw).

Eye–head coupling is reduced and context dependent after vestibular loss

Each animal's capacity to stabilize gaze was next assessed by calculating slow-phase eye-head gain, defined as the best-fit linear slope between eye and head velocity for each stride along each axis after excluding gaze reorientation events. Although the instantaneous ratio between eye and head velocity varied across the gait cycle (examples shown in Fig. 3*C*, Fig. S3*C*), it was consistently lower in BVL than in normal animals during both treadmill and overground locomotion (Fig. 3*D*, Fig. S3*D*; all

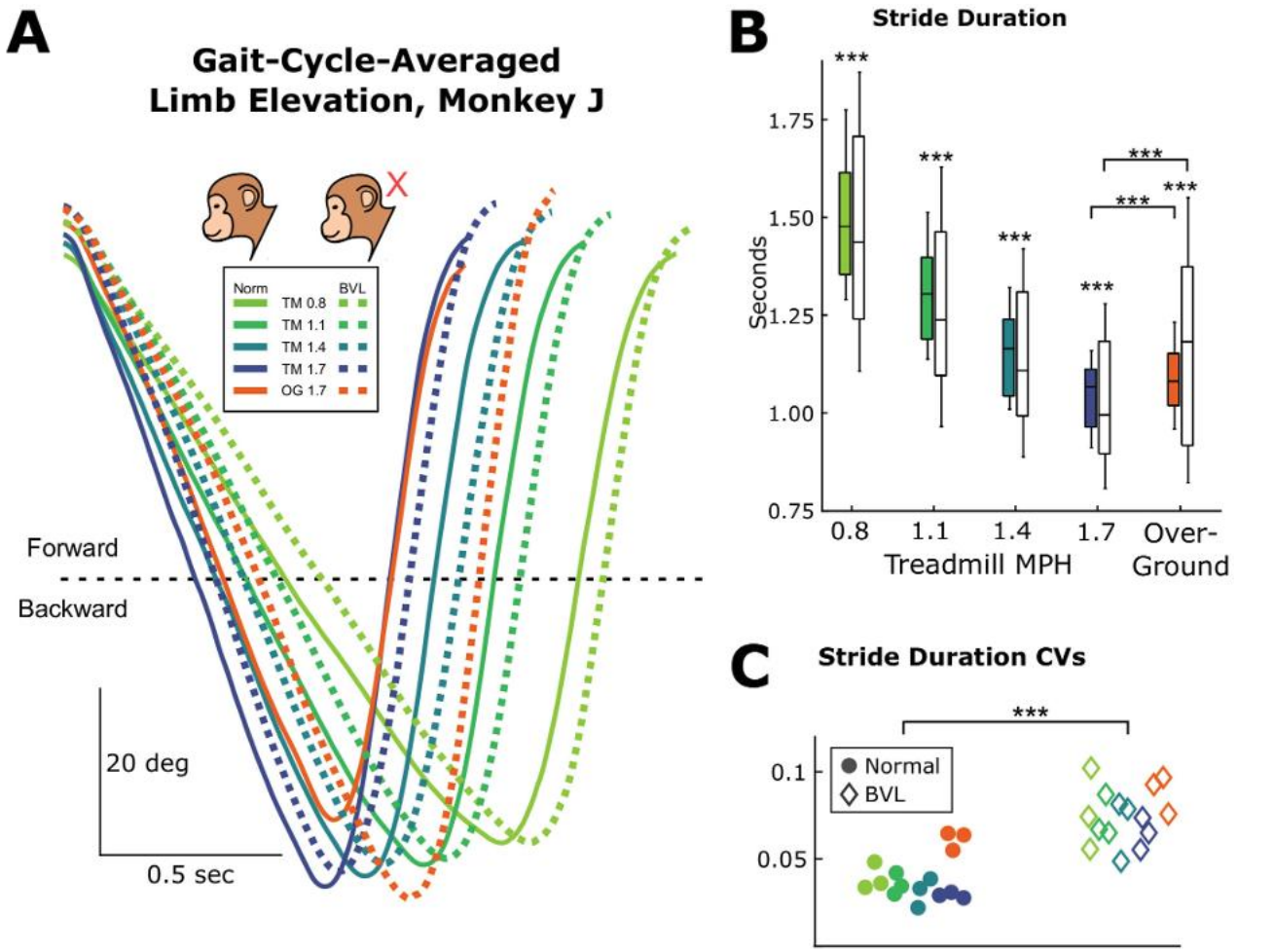

Figure 2. BVL increases limb duration variability. ***A***, Illustration of gait cycle-limb elevation for Animal J before and after BVL (solid and dotted lines, respectively). ***B***, BVL animals took shorter-duration strides than normal animals on average during treadmill walking, but vice versa during overground walking, as BVL animal stride duration increases significantly in the overground condition. ***C***, Coefficient of variation (CV) was significantly greater in BVL animals $^{**}p < 0.01$, $^{***}p < 0.001$; see Table 1 for details.

$p < 1 \times 10^{-20}$; Table 1), with no clear dependence on treadmill speed within either group. Locomotor context exerted opposite effects on gain in normal versus BVL animals. In BVL animals, gain was higher during overground walking than during treadmill locomotion ($p = 1.8 \times 10^{-2}$ for pitch; $p = 3.8 \times 10^{-10}$ for yaw), whereas in normal animals, gain was selectively reduced in the pitch axis during overground locomotion ($p = 1.6 \times 10^{-23}$). This axis-specific reduction was accompanied by a negative offset in pitch gaze velocity during overground walking (Fig. 3*A*; compare orange and blue solid traces), potentially reflecting the influence of visual motion cues arising from forward movement through the environment.

Vestibular loss increases eye–head gain variability and impairs stabilization across frequencies

As with our analysis of limb motion above, we next sought to better understand the effects of vestibular loss on gaze stabilization by quantifying stride-to-stride variability. In contrast to limb kinematics, variability in slow-phase gaze velocity did not differ significantly between groups, as reflected by comparable stride-to-stride CV between normal and BVL animals for MAV. Because MAV reflects net gaze motion (the combined effect of eye and head movements, which could in theory change independently), similar MAV variability does not inherently imply preserved eye-head coordination. Consistent with this distinction, CV across gain values fit from each stride was significantly elevated in BVL animals for both pitch and yaw axes ($p = 1.9 \times 10^{-4}$ and $p = 6.5 \times 10^{-6}$, respectively), indicating reduced consistency in the eye-head relationship following vestibular loss. Further analysis indicated that this change resulted specifically from the reduction in average gain, as gain standard deviations were similar across groups and conditions (Fig. S4*A*). This implies the increase in CV resulted from a reduction in overall gain that was not accompanied by reduced absolute variability as might have been expected if vestibular loss acted as a simple linear scaling of the entire gain distribution. Thus, although overall gaze velocity variability was comparable across groups, vestibular loss selectively destabilized the coupling between eye and head motion across locomotor conditions and axes. We next estimated gain and phase using cross-power spectral density analysis (see Materials and Methods) and found consistent group differences over the 0–5 Hz range. Specifically, across both speed-matched conditions and lower treadmill speeds, pitch gain was higher in normal (Fig. 3*E*,*F*; Fig. S4*B*), while yaw gain was likewise higher and accompanied by more compensatory phase values (closer to 180°) in normal animals over the same frequency range (Figs. S3*E*,*F*, S4*C*). Statistical comparisons for each condition are summarized in Table 1, and slow-phase gaze MAV and eye-head gain values for individual animals are shown in Figure S5. Together, these results demonstrate that

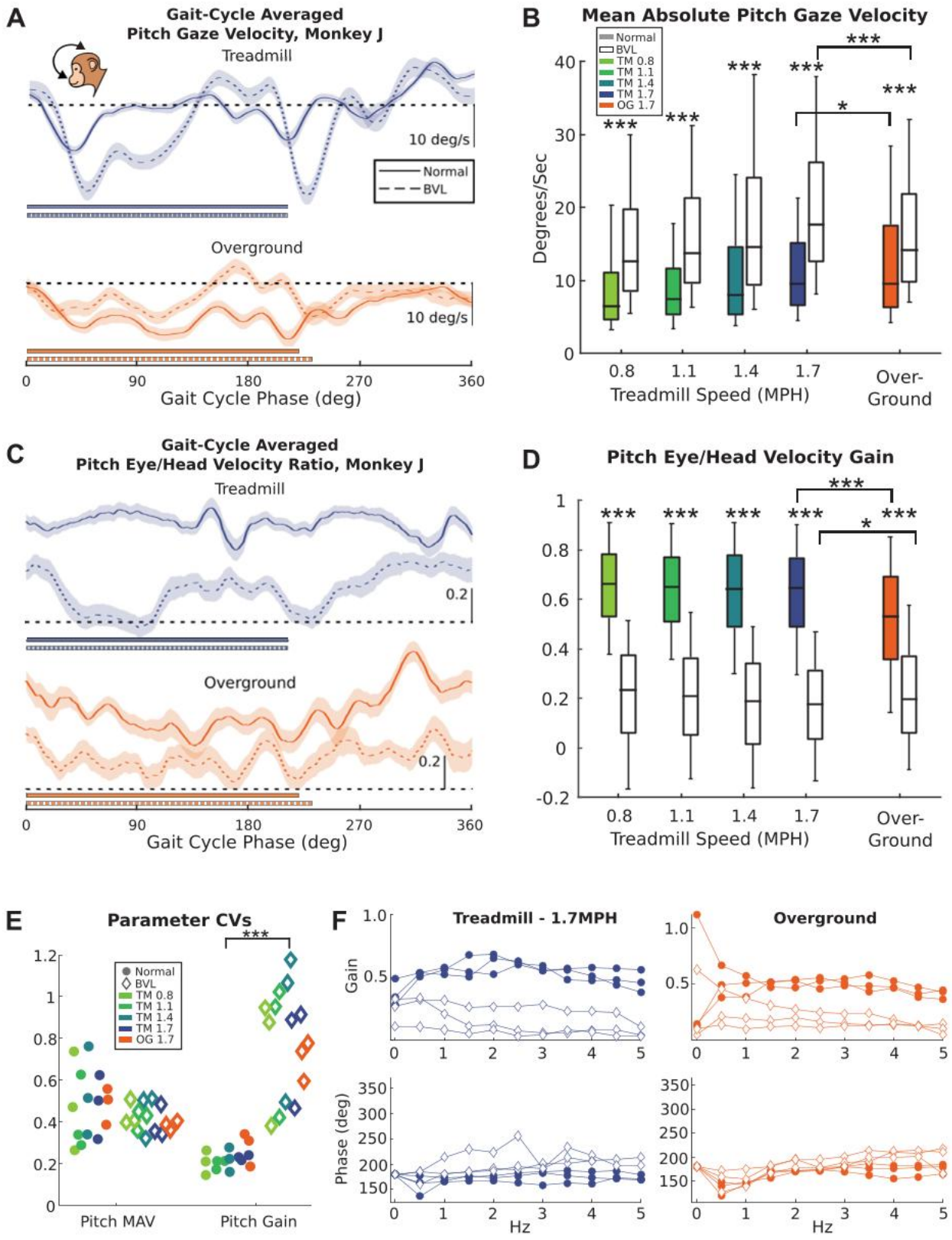

Figure 3. Slow-phase gaze stabilization during locomotion is profoundly disrupted by vestibular loss-pitch axis. ***A***, Gait cycle-averaged slow-phase pitch-axis gaze velocity for Animal J before (solid lines) and after (dashed) induction of BVL, in 1.7 MPH treadmill (top, blue traces) and overground (bottom, orange traces) conditions. Central lines and shaded regions illustrate mean ± standard error. Colored bars below traces show the portion of the gait cycle occupied by stance in each condition. ***B***, Mean absolute velocity (MAV) in the pitch axis increased in both groups with greater treadmill speed and was greater for BVL animals in all conditions. It was reduced in overground walking relative to speed-matched treadmill walking for BVL animals, but vice versa for normal animals. ***C***, As in ***A*** but illustrating gait cycle-averaged ratio between eye and head velocity. ***D***, Pitch-axis gain, determined by linear fit between head and slow-phase eye velocity within each gait cycle, was significantly higher in normal animals in every condition. It was increased in overground walking relative to speed-matched treadmill walking for BVL animals, but vice versa for normal animals. ***E***, CV was significantly higher in BVL animals (squares) than normal animals (circles) for pitch gain but not MAV. ***F***, Normal animals (filled circles) exhibited higher gains than BVL animals (unfilled diamonds) across the 0–5 Hz range (top row) in both speed-matched conditions, while phase was not as well separated. *$p < 0.05$; ***$p < 0.001$; see Table 1 for details.

Table 1. Holm–Bonferroni corrected *p* values, Figures 2–4 and Fig. S3

Comparison	0.8 MPH Norm vs BVL	1.1 MPH Norm vs BVL	1.4 MPH Norm vs BVL	1.7 MPH Norm vs BVL	Overground Norm vs BVL	1.7 MPH vs Overground, Norm	1.7 MPH vs Overground, BVL
Stride duration	$***3.7\times10^{-37}$	$***8.0\times10^{-41}$	$***1.6\times10^{-54}$	$***9.4\times10^{-41}$	$***6.5\times10^{-105}$	$***1.7\times10^{-25}$	$***1.3\times10^{-88}$
Duration CV	$***2.4\times10^{-7}$						
Pitch MAV	$***8.7\times10^{-37}$	$***7.7\times10^{-38}$	$***3.0\times10^{-38}$	$***5.1\times10^{-65}$	$***2.1\times10^{-9}$	*0.015	$***7.3\times10^{-18}$
Pitch CV	0.43						
Yaw MAV	$***3.7\times10^{-95}$	$***9.0\times10^{-112}$	$***5.9\times10^{-116}$	$***5.7\times10^{-164}$	$***9.9\times10^{-46}$	$*1.0\times10^{-2}$	$***2.2\times10^{-26}$
Yaw CV	0.72						
Pitch gain	$***2.7\times10^{-261}$	$***3.3\times10^{-279}$	$***4.4\times10^{-311}$	$***2.3\times10^{-283}$	$***4.8\times10^{-132}$	$***1.6\times10^{-23}$	$*1.8\times10^{-2}$
Pitch gain CV	$***1.9\times10^{-4}$						
Yaw gain	***∼0	***∼0	***∼0	$***5.7\times10^{-321}$	$***6.3\times10^{-189}$	7.2×10^{-1}	$***3.8\times10^{-10}$
Yaw gain CV	$***6.5\times10^{-6}$						
Reorienting rate	>1	0.76	>1	0.47	>1	$***6.8\times10^{-15}$	$***1.2\times10^{-19}$
Reorienting Magnitude	$***3.0\times10^{-54}$	$***4.2\times10^{-45}$	$***9.2\times10^{-38}$	$***1.5\times10^{-31}$	$***5.1\times10^{-11}$	$***5.1\times10^{-11}$	$***2.0\times10^{-31}$

For each parameter of interest, a linear mixed-effects model was fitted as described in the Materials and Methods section, and significance was then computed using the resulting coefficients and covariances using MATLAB's "coeftest" function. The units of analysis were reorienting events for reorienting magnitude, coefficients of variation calculated per-animal-per-condition for CV comparisons, and strides for all other comparisons.

vestibular loss selectively disrupts the consistency and temporal coordination of eye-head coupling during locomotion, despite preserved slow-phase gaze velocity variability.

Gaze reorientation timing and magnitude are altered following vestibular loss

Whereas the preceding analyses focused on continuous slow-phase gaze stabilization, we next examined discrete gaze reorientation events. Periods of rapid gaze reorientation were identified (see Materials and Methods), and their timing relative to the gait cycle was analyzed. Mean probability of reorientation across the gait cycle is shown for an example animal in Figure 4*A*. We calculated an entropy-based PLI out of a maximum of 1, as described in Kajikawa and Hackett (2005) (see Materials and Methods). Comparison of reorientation onset timing showed no significant phase locking to the gait cycle, i.e., no PLI values above chance levels (Fig. 4*B*, Table 2). This differs from prior reports of phasic modulation of gaze behavior during walking in vestibular-normal animals (Zubair et al., 2019), which may reflect differences in locomotor context, task structure, or analytic approach (see Discussion). Reorientation frequency, measured as events per second, did not differ between normal and BVL animals within any given locomotor context (Fig. 4*C*) but was significantly higher in both groups during overground walking compared with speed-matched treadmill locomotion ($p = 6.8\times10^{-15}$ for normal; $p = 1.2\times10^{-19}$ for BVL). In contrast, reorientation magnitude, quantified as the total angular displacement of each event, was modestly but significantly greater in BVL animals across treadmill speeds (Fig. 4*D*; all $p < 1\times10^{-20}$; Table 1) and smaller in BVL animals during overground locomotion ($p = 5.1\times10^{-11}$). Statistical comparisons for each condition are summarized in Table 1, and gaze reorientation rate and magnitude values for individual animals are shown in Figure S6.

Oculomotor modeling supports a reduced-precision gaze control strategy after vestibular loss

The preceding results raised two related questions: whether the increased gain variability observed after vestibular loss could be explained by a simple reduction in peripheral vestibular input, and whether existing models of rapid gaze reorientation could account for the observed changes in reorientation behavior. To address these questions, we implemented a previously established computational model of the VOR pathway that transforms head velocity into eye movements through peripheral vestibular afferents, central vestibular neurons, a neural integrator, and the oculomotor plant (Mackrous et al., 2020; Fig. 5*A*, blue box). Because experiments were performed in the light, the model also incorporated an optokinetic component to account for visual feedback based on retinal slip (see Materials and Methods).

When our recorded head kinematics were used as model input, tuning of the overall vestibular input gain allowed the model to reproduce the mean slow-phase eye movements observed in both vestibular-normal and BVL animals (Fig. 5*B*). However, reducing vestibular gain alone led to a decrease in output gain variability, opposite to the empirical observation that BVL animals exhibit lower mean gain together with higher gain CV. To resolve this discrepancy, we introduced an additional noise source at the junction between vestibular afferents and vestibular nuclei (Fig. 5*A*, green shaded box), implemented as additive Gaussian noise consistent with spontaneous afferent variability (Goldberg, 2000). Importantly, this modification introduced only a single additional noise parameter and was not independently tuned across locomotor conditions, ensuring that the observed changes in gain variability did not arise from condition-specific overfitting. With this modification, reductions in vestibular input gain were accompanied by increased stride-to-stride variability in modeled eye-head gain (Fig. 5*C*), qualitatively reproducing the pattern observed in macaques following vestibular loss. Model parameters were estimated independently for each animal and locomotor condition using the same fitting procedure, and the addition of a single noise term was the minimal modification required to account for the observed dissociation between mean gain and gain variability.

We next extended the model to account for gaze reorientation behavior by incorporating a previously proposed computational framework for quick-phase generation, in which gaze error estimated from eye and head motion triggers a corrective movement when an internal quick-phase ("Q") threshold is exceeded (Chun and Robinson, 1978; Fig. 5*A*, red box, threshold indicated in orange shaded box). Model parameters were fit separately for each animal and locomotor condition using a subset of empirically identified reorientation events which excluded those assumed to be saccades (see Materials and Methods). This analysis revealed significantly elevated yaw axis thresholds in BVL animals relative to controls (Fig. 5*D*; $p = 9.6\times10^{-6}$), indicating that BVL animals tolerated larger gaze position errors before initiating corrective reorientations. The absence of a significant pitch-axis threshold difference ($p = 0.10$) may reflect additional

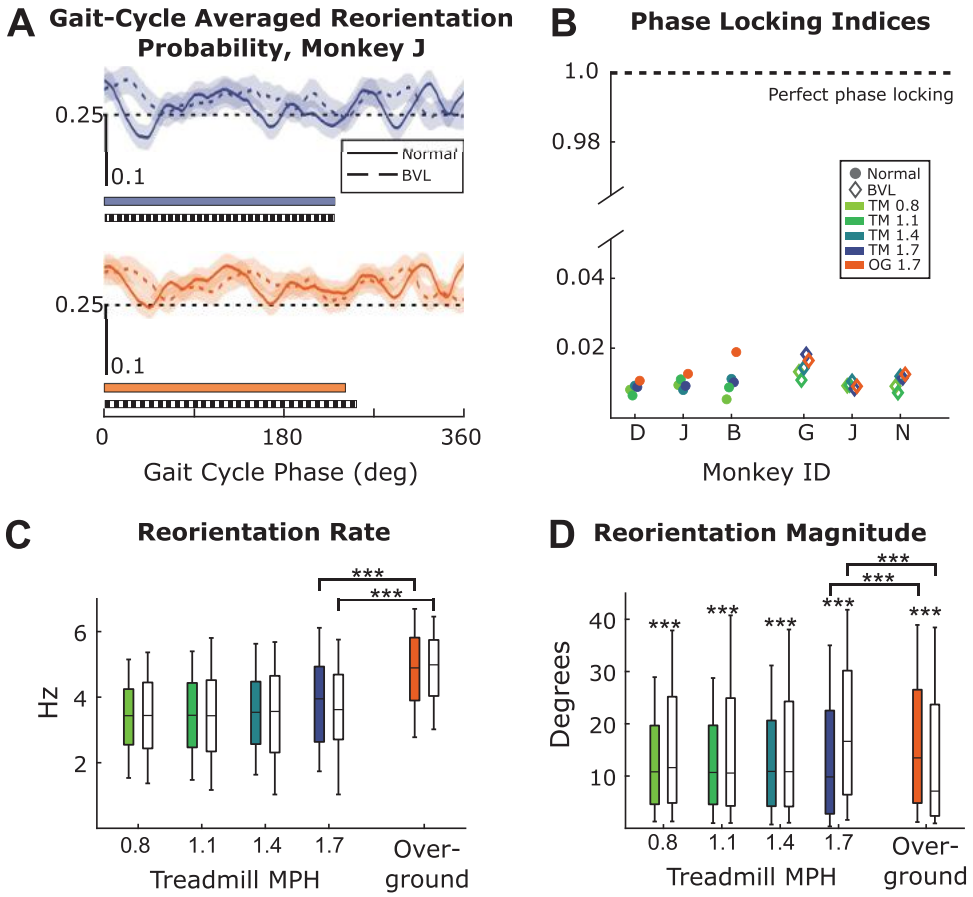

Figure 4. Characteristics of gaze reorientation during locomotion. ***A***, Gait cycle-averaged probability of reorienting event occurrence in Animal J before (solid lines) and after (dashed) induction of BVL, in 1.7 MPH treadmill (top, blue traces) and overground (top, orange traces) conditions. Central lines and shaded regions illustrate mean ± standard error. Colored bars below traces show the portion of the gait cycle occupied by stance phase in each condition. ***B***, Prevalence of phase locking was assessed using the entropy of gaze reorientation timing distributions, out of a maximum of 1.0. Relative to chance distributions computed from reshuffled interphase intervals, no significant phase locking was found (Table 2). ***C***, The overall frequency of reorienting events did not differ between the two groups and was higher in both groups in the overground condition relative to speed-matched treadmill walking (Table 1). ***D***, Reorientation magnitude was larger in BVL animals during treadmill locomotion but smaller in the overground condition. Size increased for normal animals, but reduced for BVL, in overground walking compared with 1.7 MPH treadmill (Table 1). ***$p < 0.001$.

Table 2. Holm–Bonferroni corrected *p* values and phase locking indices, Figure 4*A*

		Walking condition									
		0.8 MPH treadmill		1.1 MPH treadmill		1.4 MPH treadmill		1.7 MPH treadmill		Overground	
Animal	Vestibular condition	*p*	PLI	*p*	PLI	*p*	PLI	*p*	PLI	*p*	PLI
D	Normal	$p > 1$	0.014	$p > 1$	0.018	$p > 1$	0.017	$p > 1$	0.027	$p > 1$	0.013
J		$p > 1$	0.018	$p = 0.92$	0.022	$p > 1$	0.017	$p > 1$	0.023	$p > 1$	0.018
B		$p > 1$	0.010	$p > 1$	0.010	$p > 1$	0.012	$p > 1$	0.017	$p > 1$	0.055
G	Bilateral vestibular loss	$p > 1$	0.030	$p > 1$	0.025	$p > 1$	0.026	$p > 1$	0.042	$p > 1$	0.034
J		$p > 1$	0.015	$p > 1$	0.017	$p > 1$	0.022	$p = 0.36$	0.016	$p > 1$	0.019
N		$p = 0.36$	0.012	>1	0.021	$p > 1$	0.022	$p > 1$	0.026	$p > 1$	0.029

Phase locking indices (PLIs) were calculated using distributional entropy. Significance was determined via bootstrapping 20,000 alternative phase distributions using shuffled interphase intervals.

visual motion influences present during forward locomotion. Together, these results indicate that vestibular loss alters the threshold for triggering gaze reorientations, allowing larger gaze errors to accumulate before corrective movements are initiated.

Discussion

Our results provide the first systematic characterization of locomotor gaze control in primates with chronic BVL. Although vestibular contributions to gaze stabilization are well characterized in stationary, head-fixed, and passive motion paradigms, their role during natural primate locomotion remains poorly understood. This gap is particularly relevant given that locomotion generates phasic head movements across species (Solomon and Cohen, 1992; Cromwell et al., 2004; Kavanagh et al., 2006; Dunbar et al., 2008; Xiang et al., 2008; Zubair et al., 2016; Zubair et al., 2019; Wei et al., 2026). By directly comparing macaques with BVL to controls during self-paced overground walking and across multiple treadmill speeds, we show that vestibular input shapes gaze behavior during locomotion across both slow-phase stabilization and rapid gaze reorientation. BVL produced consistent gaze control deficits, including greater

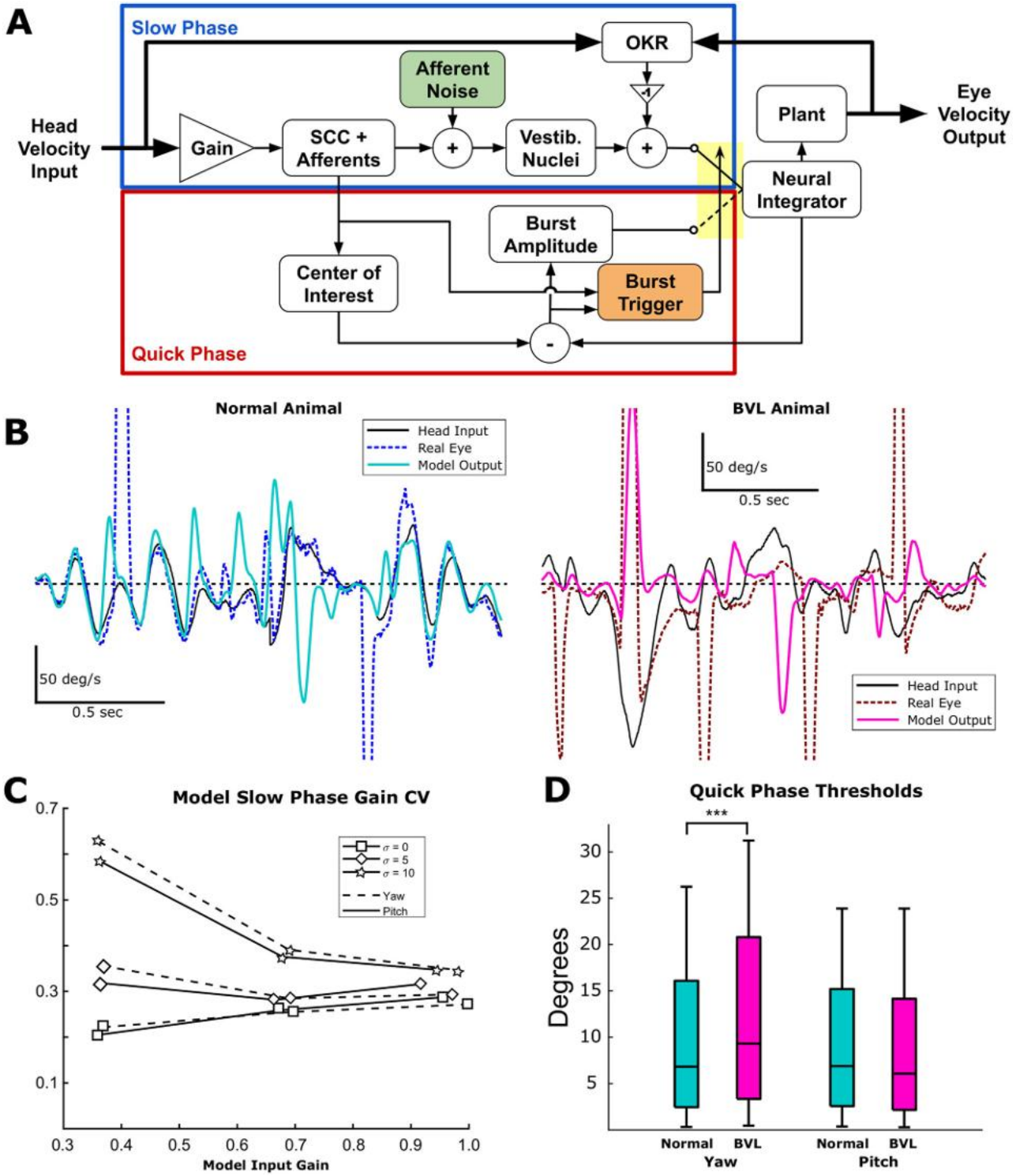

Figure 5. Modeling of eye movement generation. ***A***, Block diagram of oculomotor pathway model. Head velocity is multiplied by an input gain and processed to produce a modeled eye velocity output. Slow-phase eye movement generation (blue box) includes transfer functions representing the semicircular canals and afferents, vestibular nuclei, optokinetic reflex (OKR), and neural integrator. Spontaneous afferent activity is represented by Gaussian noise at the input to the vestibular nuclei. Quick-phase generation (red box) compares a head velocity-dependent "center of interest" to eye movement commands from the neural integrator to determine size and timing of a reorienting movement. When this difference exceeds a head velocity-dependent level (*Q*-threshold), the model switches states (yellow box) and a quick phase is triggered. Resulting commands are passed through a transfer function representing the eye plant. Specific parameters and transfer functions are listed in the Materials and Methods section. ***B***, Example output from the model applied to normal (left) and BVL (right) animal head movements, with input gain set to best match each animal's slow-phase eye velocity. ***C***, In the absence of noise, CV and gain of model eye velocity output were positively correlated, rather than negatively as was observed empirically. ***D***, Fitting of quick-phase generation parameter to data from normal versus BVL animals suggests greater error tolerance in the second group in the yaw axis ($p = 9.6 \times 10^{-6}$). The predominantly vertical orientation of optic flow during locomotion may confound underlying vestibular differences in pitch.

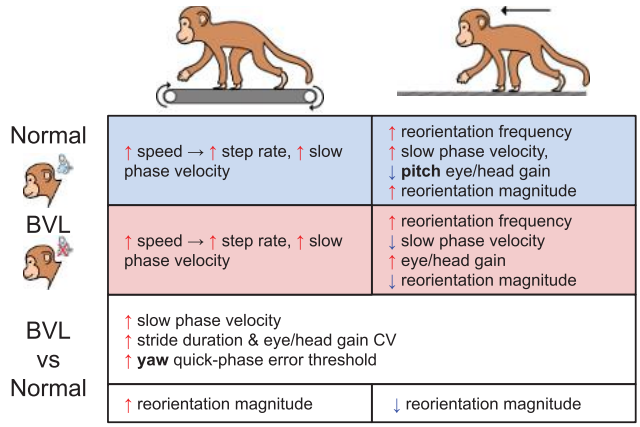

Figure 6. Summary of findings. Comparison of key results either across treadmill speeds (left column, top two rows), in overground as compared with speed-matched treadmill (right column, top two rows), or between BVL and normal animals in those paradigms (bottom rows).

slow-phase gaze movements, reduced and noisier compensatory gains, and altered gaze-reorienting movement sizes. Together, these findings, summarized in Figure 6, demonstrate that vestibular input is essential for both gaze stabilization and reorientation during locomotion and that its loss drives a fundamental system-level recalibration of locomotor gaze control.

Adaptive strategies and recalibration after vestibular loss

A central question in systems neuroscience is how the brain adapts movement strategies when key sensorimotor reflexes supporting postural and gaze stabilization are chronically absent. During locomotion, this problem is especially challenging because head movements are rapid, rhythmic, and self-generated. Although visual and proprioceptive feedback can contribute to compensation after vestibular loss, their processing delays limit their ability to stabilize gaze against stride-linked head motion directly. Thus, residual gaze stabilization following BVL likely depends on predictive motor signals, including efference-copy-based estimates of the sensory consequences of active head movements. This interpretation is supported by neurophysiological recordings from vestibular pathways in rhesus monkeys showing that compensation after vestibular loss involves enhanced sensitivity to proprioceptive and motor-related signals (Sadeghi et al., 2010, 2011, 2012; Jamali et al., 2014). These studies revealed increased responses to passively activated neck proprioceptive inputs after vestibular loss and dynamic regulation of efference-copy signals during active head movements. Together, these findings provide a neural correlate for improved gaze stability during active self-motion after vestibular loss in patients and rhesus monkeys (Dichgans et al., 1973; Newlands et al., 2001; Della Santina et al., 2002). Accordingly, the improved gaze stabilization we observed during self-paced overground walking may reflect greater engagement of internally generated motor predictions and proprioceptive feedback.

Optimal cue integration theory posits that the brain combines inputs by weighting each according to its reliability (Ernst and Banks 2002; Körding and Wolpert, 2004; Cheng et al., 2007; Angelaki et al., 2009; Clemens et al., 2011). When vestibular reliability is reduced, this framework predicts that other cues should be upweighted. Consistent with this view, individuals with vestibular loss show increased reliance on proprioception (Goodworth and Peterka, 2010; Peterka et al., 2011), and cortical neurons dynamically adjust their responses to changes in visual-vestibular cue reliability in a manner consistent with optimal integration (Angelaki et al., 2009; Fetsch et al., 2011). Thus, compensation after vestibular loss may reflect both predictive motor control and reliability-based recalibration of remaining sensory cues.

Together, these findings suggest that chronic vestibular loss drives systematic reweighting toward visual and proprioceptive cues while also reshaping the criteria used to trigger gaze-reorienting movements. One striking observation was that BVL monkeys exhibited elevated thresholds for triggering rapid gaze reorientations, which would otherwise be expected to occur more frequently given their unstable head motion. Because visual input is transiently suppressed during saccades and quick phases to prevent perception of retinal blur (reviewed in Sun and Goldberg, 2016; Wurtz, 2018), increasing these thresholds may help preserve visual access to the environment at the expense of precise gaze placement. Although we did not directly measure the neural correlates of these thresholds, our modeling showed that elevated gaze-error tolerance was sufficient to account for altered reorientation statistics following vestibular loss. Consistent with this interpretation, elevated thresholds were associated with larger reorientation magnitudes, suggesting increased gaze error. In contrast, reorientation magnitudes were reduced during self-paced overground walking, where slow-phase stabilization improved in BVL animals. Thus, adaptation after vestibular loss involves not only sensory reweighting but also adjustment of the criteria governing gaze reorientation. We predict that under conditions of reduced proprioceptive reliability, such as locomotion on compliant surfaces (Zobeiri et al., 2021; Zobeiri et al., 2022), or heightened visual demands, such as obstacle-rich environments, the limits of this compensatory strategy will become apparent, requiring further adaptations in gaze or locomotor control.

By augmenting a Robinson-style model (reviewed in Robinson, 2022) to include intrinsic sensorimotor noise and adjustable gaze-error thresholds, we reproduced both the increased slow-phase gain variability and the consistent frequency of gaze reorientations observed in BVL animals. The noise term captured the heightened trial-to-trial variability characteristic of vestibular loss, consistent with the view that sensorimotor variability must be represented to understand self-motion perception and oculomotor behavior (Cousins et al., 2013; Nouri and Karmali, 2018; Glasauer and Straka, 2022). Reproducing the BVL data also required elevated gaze-error thresholds, consistent with a precision-stability tradeoff that tolerates imprecise gaze placement to reduce gaze resets and preserve continuous visual input. Accordingly, vestibular loss does not simply reduce reflex gain but induces a recalibration of oculomotor control in which compensation emerges through coordinated changes in sensory weighting and error tolerance rather than uniform scaling of reflex pathways.

Locomotor context shapes gaze control

Our data reveal that gaze control is strongly shaped by locomotor context. For example, contrasting with prior work showing strong gait-linked coupling during navigation of irregular terrain (Zubair et al., 2019), here neither group showed strong phase locking. Because our environments likely imposed minimal demands on foot placement precision, stronger gaze-stride coupling may emerge only when terrain complexity makes visual guidance of upcoming footfall locations behaviorally critical (Matthis et al., 2018).

Slow-phase stabilization was also context dependent. Normal animals exhibited reduced pitch-axis gain during overground walking relative to treadmill locomotion. This likely reflects enhanced optic flow and/or tracking of specific targets during forward displacement through the environment, which is absent during treadmill locomotion (Solomon and Cohen, 1992; Muller et al., 2023). Because forward locomotion generates predominantly vertical optic flow (aligned with pitch-axis motion), this substitution effect would be expected to manifest preferentially in that axis, consistent with our observations. Importantly, the direction of this modulation differed between groups. In control animals, optic flow during overground walking reduced reliance on vestibular input while preserving effective visual stability. In contrast, following BVL, visual and proprioceptive cues are likely upweighted (Goodworth and Peterka, 2010; Peterka et al., 2011), such that optic flow during overground locomotion permits partial restoration of slow-phase stabilization despite absent vestibular drive. Thus, overground and treadmill locomotion do not simply scale gaze control, but instead reshape the balance of visual, proprioceptive, and vestibular contributions as a function of vestibular integrity.

This redistribution of sensory weighting extends beyond the oculomotor system. We recently demonstrated that neck muscle coordination strategies for head stabilization are flexibly restructured during overground versus treadmill locomotion in primates, with overground walking engaging a distinct population-level control geometry (Wei et al., 2026). The present findings extend this principle to eye-head coordination, indicating that locomotor context reshapes muscular and oculomotor stabilization strategies. Because sensory systems are tuned to natural input statistics (Mitchell et al., 2018), greater experience with overground walking may enable more accurate motor predictions and improved performance in this condition, although input variability within strides may still alter the difficulty of gaze stabilization (MacNeilage and Glasauer, 2017). One limitation worth noting is that our quick-phase fitting relied on an assumption that reorientations in the same direction as head motion constituted quick phases, when in reality some of these would have been saccades. Emerging approaches such as head-mounted, world-facing cameras (Singh et al., 2025) will further enable quantification of gaze strategies under naturalistic conditions, helping to dissociate strategic suppression of saccades from altered triggering of reflexive quick phases.

Together, these results support a systems-level view in which head and gaze stabilization operate under locomotion-dependent control regimes rather than a fixed reflex architecture. This flexibility is likely to be particularly consequential in the context of human vestibular disease. Vestibular disorders are common and debilitating (Agrawal et al., 2013), increasing fall risk (Herdman et al., 2000; Dobbels et al., 2020), and imposing substantial cognitive and emotional burdens (MacDowell et al., 2018; Lucieer et al., 2020; Molnár et al., 2022). The elevated stride-to-stride variability observed in our BVL macaques closely mirrors that reported in patients with bilateral vestibulopathy during both treadmill (McCrum et al., 2019) and overground walking (Schniepp et al., 2012; Wuehr et al., 2016), demonstrating that fundamental locomotor instability following vestibular loss is conserved across species. This cross-species similarity underscores the translational value of the primate BVL model, which enables study of naturalistic locomotor behavior alongside access to underlying neural circuitry. Together, these findings establish quantitative behavioral benchmarks directly linking vestibular dysfunction to sensorimotor control principles and demonstrate that chronic vestibular loss does not simply degrade gaze stability but reorganizes the strategies governing eye-head coordination during self-motion.

References

Agrawal Y, Ward BK, Minor LB (2013) Vestibular dysfunction: prevalence, impact and need for targeted treatment. J Vestib Res 23:113–117.

Angelaki DE, Gu Y, DeAngelis GC (2009) Multisensory integration: psychophysics, neurophysiology, and computation. Curr Opin Neurobiol 19: 452–458.

Anson ER, Kiemel T, Carey JP, Jeka JJ (2017) Eye movements are correctly timed during walking despite bilateral vestibular hypofunction. J Assoc Res Otolaryngol 18:591–600.

Boisgontier MP, Cheval B (2016) The anova to mixed model transition. Neurosci Biobehav Rev 68:1004–1005.

Cheng K, Shettleworth SJ, Huttenlocher J, Rieser JJ (2007) Bayesian integration of spatial information. Psychol Bull 133:625–637.

Chun KS, Robinson DA (1978) A model of quick phase generation in the vestibuloocular reflex. Biol Cybern 28:209–221.

Clemens IAH, De Vrijer M, Selen LPJ, Van Gisbergen JAM, Pieter Medendorp W (2011) Multisensory processing in spatial orientation: an inverse probabilistic approach. J Neurosci 31:5365–5377.

Corneil BD, Olivier E, Munoz DP (2002) Neck muscle responses to stimulation of monkey superior colliculus. I. Topography and manipulation of stimulation parameters. J Neurophysiol 88:1980–1999.

Courtine G, Roy RR, Hodgson J, McKay H, Raven J, Zhong H, Yang H, Tuszynski MH, Edgerton VR (2005) Kinematic and EMG determinants in quadrupedal locomotion of a non-human primate (rhesus). J Neurophysiol 93:3127–3145.

Cousins S, Kaski D, Cutfield N, Seemungal B, Golding JF, Gresty M, Glasauer S, Bronstein AM (2013) Vestibular perception following acute unilateral vestibular lesions. PLoS One 8:e61862.

Cromwell R, Schurter J, Shelton S, Vora S (2004) Head stabilization strategies in the sagittal plane during locomotor tasks. Physiother Res Int 9:33–42.

Cullen KE (2019) Vestibular processing during natural self-motion: implications for perception and action. Nat Rev Neurosci 20:346–363.

Della Santina CC, Cremer PD, Carey JP, Minor LB (2002) Comparison of head thrust test with head autorotation test reveals that the vestibulo-ocular reflex is enhanced during voluntary head movements. Arch Otolaryngol Head Neck Surg 128:1044–1054.

Dichgans J, Bizzi E, Morasso P, Tagliasco V (1973) Mechanisms underlying recovery of eye-head coordination following bilateral labyrinthectomy in monkeys. Exp Brain Res 18:548–562.

Dobbels B, et al. (2020) Prospective cohort study on the predictors of fall risk in 119 patients with bilateral vestibulopathy. PLoS One 15: e0228768.

Dunbar DC, Macpherson JM, Simmons RW, Zarcades A (2008) Stabilization and mobility of the head, neck and trunk in horses during overground locomotion: comparisons with humans and other primates. J Exp Biol 211:3889–3907.

Ernst MO, Banks MS (2002) Humans integrate visual and haptic information in a statistically optimal fashion. Nature 415:429–433.

Fernandez C, Goldberg JM (1971) Physiology of peripheral neurons innervating semicircular canals of the squirrel monkey. II. Response to sinusoidal stimulation and dynamics of peripheral vestibular system. J Neurophysiol 34:661–675.

Fetsch CR, Pouget A, DeAngelis GC, Angelaki DE (2011) Neural correlates of reliability-based cue weighting during multisensory integration. Nat Neurosci 15:146–154.

Glasauer S, Straka H (2022) Low gain values of the vestibulo-ocular reflex can optimize retinal image slip. Front Neurol 13:897293.

Goldberg JM (2000) Afferent diversity and the organization of central vestibular pathways. Exp Brain Res 130:277–297.

Goldberg JM, Wilson VJ, Cullen KE, Angelaki DE (2011) *The vestibular system: a sixth sense*. Oxford, England: Oxford University Press.

Goodworth AD, Peterka RJ (2010) Influence of bilateral vestibular loss on spinal stabilization in humans. J Neurophysiol 103:1978–1987.

Helling K, Schönfeld U, Clarke AH (2007) Treatment of Ménière's disease by low-dosage intratympanic gentamicin application: effect on otolith function. Laryngoscope 117:2244–2250.

Herdman SJ, Blatt P, Schubert MC, Tusa RJ (2000) Falls in patients with vestibular deficits. Am J Otol 21:847–851.

Imai T, Moore ST, Raphan T, Cohen B (2001) Interaction of the body, head, and eyes during walking and turning. Exp Brain Res 136:1–18.
Jamali M, Mitchell DE, Dale A, Carriot J, Sadeghi SG, Cullen KE (2014) Neuronal detection thresholds during vestibular compensation: contributions of response variability and sensory substitution. J Physiol 592:1565–1580.
Kajikawa Y, Hackett TA (2005) Entropy analysis of neuronal spike train synchrony. J Neurosci Methods 149:90–93.
Kavanagh J, Barrett R, Morrison S (2006) The role of the neck and trunk in facilitating head stability during walking. Exp Brain Res 172:454–463.
Körding KP, Wolpert DM (2004) Bayesian integration in sensorimotor learning. Nature 427:244–247.
Lucieer FMP, Van Hecke R, van Stiphout L, Duijn S, Perez-Fornos A, Guinand N, Van Rompaey V, Kingma H, Joore M, van de Berg R (2020) Bilateral vestibulopathy: beyond imbalance and oscillopsia. J Neurol 267:241–255.
MacDowell SG, Wellons R, Bissell A, Knecht L, Naquin C, Karpinski A (2018) The impact of symptoms of anxiety and depression on subjective and objective outcome measures in individuals with vestibular disorders. J Vestib Res 27:295–303.
Mackrous I, Carriot J, Cullen KE, Chacron MJ (2020) Neural variability determines coding strategies for natural self-motion in macaque monkeys. Elife 9:e57484.
MacNeilage PR, Glasauer S (2017) Quantification of head movement predictability and implications for suppression of vestibular input during locomotion. Front Comput Neurosci 11:47.
Mathis A, Mamidanna P, Cury KM, Abe T, Murthy VN, Mathis MW, Bethge M (2018) Deeplabcut: markerless pose estimation of user-defined body parts with deep learning. Nat Neurosci 21:1281–1289.
Matthis JS, Yates JL, Hayhoe MM (2018) Gaze and the control of foot placement when walking in natural terrain. Curr Biol 28:1224–1233.e5.
McCrum C, Lucieer F, van de Berg R, Willems P, Fornos AP, Guinand N, Karamanidis K, Kingma H, Meijer K (2019) The walking speed-dependency of gait variability in bilateral vestibulopathy and its association with clinical tests of vestibular function. Sci Rep 9:18392.
Millar JL, Zobeiri OA, Souza WH, Schubert MC, Cullen KE (2023) Head movement kinematics are differentially altered for extended versus short duration gait exercises in individuals with vestibular loss. Sci Rep 13:16213.
Mitchell DE, Kwan A, Carriot J, Chacron MJ, Cullen KE (2018) Neuronal variability and tuning are balanced to optimize naturalistic self-motion coding in primate vestibular pathways. Elife 7:e43019.
Molnár A, Maihoub S, Mavrogeni P, Tamás L, Szirmai Á (2022) Depression scores and quality of life of vertiginous patients, suffering from different vestibular disorders. Eur Arch Otorhinolaryngol 279:5173–5179.
Muller KS, Matthis J, Bonnen K, Cormack LK, Huk AC, Hayhoe M (2023) Retinal motion statistics during natural locomotion. Elife 12:e82410.
Newlands SD, Hesse SV, Haque A, Angelaki DE (2001) Head unrestrained horizontal gaze shifts after unilateral labyrinthectomy in the rhesus monkey. Exp Brain Res 140:25–33.
Nouri S, Karmali F (2018) Variability in the vestibulo-ocular reflex and vestibular perception. Neuroscience 393:350–365.
Peterka RJ, Statler KD, Wrisley DM, Horak FB (2011) Postural compensation for unilateral vestibular loss. Front Neurol 2:57.
Robinson DA (2022) David A. Robinson's modeling the oculomotor control system. In: *Progress in brain research* (Anastasio TJ, Demer JL, John Leigh R, Luebke AE, John van Opstal A, Optican LM, Ramat S, Zee D, eds), Vol 267, pp 15–249. Netherlands: Elsevier B.V.
Sadeghi SG, Minor LB, Cullen KE (2010) Neural correlates of motor learning in the vestibulo-ocular reflex: dynamic regulation of multimodal integration in the macaque vestibular system. J Neurosci 30:10158–10168.
Sadeghi SG, Minor LB, Cullen KE (2011) Multimodal integration after unilateral labyrinthine lesion: single vestibular nuclei neuron responses and implications for postural compensation. J Neurophysiol 105:661–673.
Sadeghi SG, Minor LB, Cullen KE (2012) Neural correlates of sensory substitution in vestibular pathways following complete vestibular loss. J Neurosci 32:14685–14695.
Scarpa A, et al. (2024) Efficacy and preservation of hearing with low-dose gentamicin in unilateral Meniere's disease: a clinical symptomatology-based study. Am J Otolaryngol 45:1.
Schniepp R, Wuehr M, Neuhaeusser M, Kamenova M, Dimitriadis K, Klopstock T, Strupp M, Brandt T, Jahn K (2012) Locomotion speed determines gait variability in cerebellar ataxia and vestibular failure. Mov Disord 27:125–131.
Scudder CA, Kaneko CS, Fuchs AF (2002) The brainstem burst generator for saccadic eye movements: a modern synthesis. Exp Brain Res 142:439–462.
Singh VP, Li J, Dawson K, Mitchell JF, Miller CT (2025) Active vision in freely moving marmosets using head-mounted eye tracking. Proc Natl Acad Sci U S A 122:e2412954122.
Solomon D, Cohen B (1992) Stabilization of gaze during circular locomotion in light. I. Compensatory head and eye nystagmus in the running monkey. J Neurophysiol 67:1146–1157.
Srivastava A, Ahmad OF, Pacia CP, Hallett M, Lungu C (2018) The relationship between saccades and locomotion. J Mov Disord 11:93.
Sun LD, Goldberg ME (2016) Corollary discharge and oculomotor proprioception: cortical mechanisms for spatially accurate vision. Ann Rev Vis Sci 2:61–84.
Takahashi M, Veale R (2023) Pathways for naturalistic looking behavior in primate I: behavioral characteristics and brainstem circuits. Neuroscience 532:133–163.
Vagvolgyi BP, Jayakumar RP, Madhav MS, Knierim JJ, Cowan NJ (2022) Wide-angle, monocular head tracking using passive markers. J Neurosci Methods 368:109453.
van Gisbergen JAM, van Opstal AJ, Schoenmakers JJM (1985) Experimental test of two models for the generation of oblique saccades. Exp Brain Res 57:321–336.
Wei RH, Stanley OR, Charles AS, Cullen KE (2026) Locomotion engages context-dependent motor strategies for head stabilization in primates. Commun Biol 9:234.
Wuehr M, Nusser E, Decker J, Krafczyk S, Straube A, Brandt T, Jahn K, Schniepp R (2016) Noisy vestibular stimulation improves dynamic walking stability in bilateral vestibulopathy. Neurology 86:2196–2202.
Wurtz RH (2018) Corollary discharge contributions to perceptual continuity across saccades. Ann Rev Vis Sci 4:215–237.
Xiang Y, Yakushin SB, Kunin M, Raphan T, Cohen B (2008) Head stabilization by vestibulocollic reflexes during quadrupedal locomotion in monkey. J Neurophysiol 100:763–780.
Yang T-H, Liu S-H, Young Y-H (2010) Evaluation of Guinea pig model for ocular and cervical vestibular-evoked myogenic potentials for vestibular function test. Laryngoscope 120:1910–1917.
Zobeiri OA, Ostrander B, Roat J, Agrawal Y, Cullen KE (2021) Loss of peripheral vestibular input alters the statistics of head movement experienced during natural self-motion. J Physiol 599:2239–2254.
Zobeiri OA, Wang L, Millar JL, Schubert MC, Cullen KE (2022) Head movement kinematics are altered during balance stability exercises in individuals with vestibular schwannoma. J Neuroeng Rehabil 19:120.
Zubair HN, Beloozerova IN, Sun H, Marlinski V (2016) Head movement during walking in the cat. Neuroscience 332:101–120.
Zubair HN, Chu KMI, Johnson JL, Rivers TJ, Beloozerova IN (2019) Gaze coordination with strides during walking in the cat. J Physiol 597:5195–5229.